Photoisomerization-Induced Melting and Spontaneous Crystallization in Acicular Star-Shaped Microcrystals.

Kevin Lam[2], Imadul Islam [1], Ebrahim Bushnak [1], Raghad Al-Muzarie [1], and Christopher J. Bardeen[*2], Rabih O. Al-Kaysi[*1]

[1] College of Science and Health Professions, King Saud bin Abdulaziz University for Health Sciences, and, King Abdullah International Medical Research Center (Nanomedicine), Ministry of National Guard Health Affairs, Riyadh 11426, Kingdom of Saudi Arabia.
[2] Department of Chemistry, University of California, Riverside, Riverside, CA 92521, USA.
* Correspondence: rabihalkaysi@gmail.com, kaysir@ksau-hs.edu.sa ; Tel.: +966561429528

Abstract:

In recent years, significant advancements have occurred in the development of smart materials, particularly in creating molecular crystals that can convert light energy into mechanical work. In this study, we focus on the synthesis, characterization, and photomechanical behavior of a new molecule, bis(2,2,2-trifluoroethyl) (E)-2-(3-(anthracen-9-yl)allylidene)malonate (**trans-ATF**), which is capable of forming acicular star-shaped microcrystals resembling sea Urchins. These crystals are formed via the seeded growth method from aqueous surfactant solution. When these microcrystals are exposed to visible light while suspended in an aqueous medium, they undergo a process in which the tips of these microcrystals temporarily become liquid and move inward towards the center. This transformation is initiated by the photoisomerization of trans-ATF to cis-ATF when absorbing visible light. After this phase, the melted crystals quickly return to their solid state in less than a minute while maintaining a balance between the two different photoisomers of the ATF molecule. In the presence of suspended silica microspheres, the star-shaped trans-ATF microcrystals undergo a similar melting process induced by visible light. During this process, the melted branches capture and pull these suspended silica microspheres towards the center of the molten crystal structure. This leads to the silica microspheres becoming enclosed within the molten crystal, which then solidifies again.

Graphical Abstract:

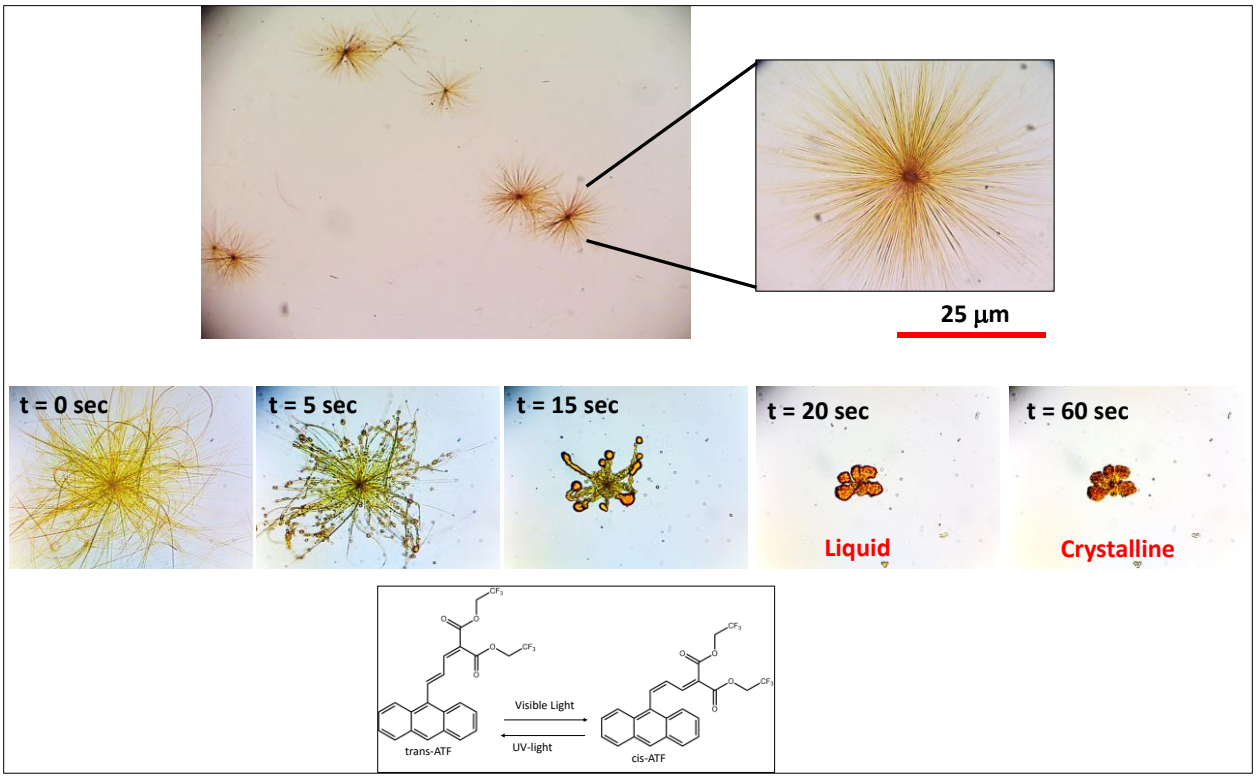

Introduction:

In recent years, a promising class of smart crystals with the remarkable ability to convert light into mechanical work has come to the forefront of scientific exploration[1–3]. This groundbreaking development was originally demonstrated independently by Irie[4] and Bardeen[5,6], who unveiled the potential of molecular crystals composed of various photochemically reactive molecules to efficiently harness photons and transform them into mechanical energy. Consequently, the scientific community has been fervently engaged in the pursuit of uncovering and synthesizing novel photomechanical molecular crystals[7–9]. Photomechanical crystals can generally be categorized into two main groups based on their behavior: those that convert light energy into mechanical work while maintaining their crystalline structure (referred to as crystal-to-crystal transformation), examples exhibit diverse responses such as jumping (photosalient)[10–14], expanding[5,15–17], bending[18–25], curling[10,26–28], peeling[29–31], or even demonstrating autonomous behaviors[32]. Additionally, there are crystals that undergo a photoinduced transition from a crystalline state to a liquid phase, a phenomenon that is particularly prominent in azobenzene derivatives[33–36]. The chemical literature is replete with numerous examples showcasing these fascinating crystals.

Our group has focused on investigating the photomechanical responses of specific molecules composed of anthracene derivatives, namely **DMAAM**, **DVAM**, and **AYAD**, which undergo reversible photoinduced

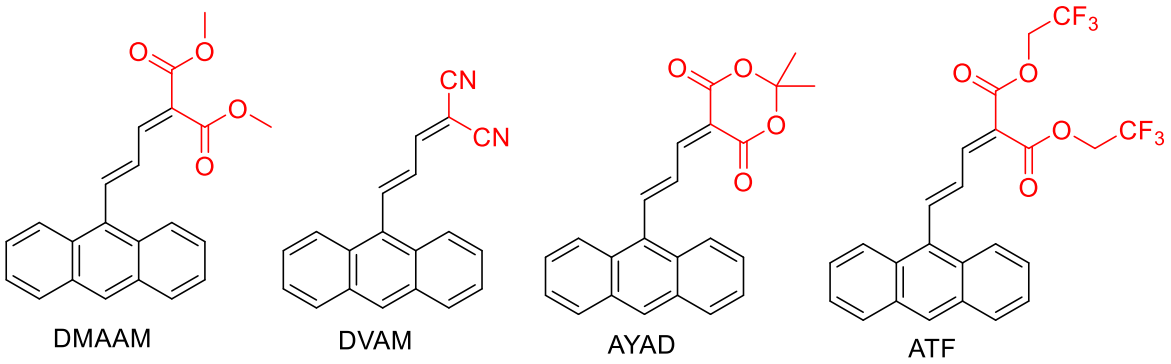

trans-to-cis isomerization around the double bond directly attached to the anthracene ring. This isomerization process serves as the driving force behind the photomechanical behavior exhibited by these crystals. While each of these derivatives displays a distinctive photomechanical behavior, **DMAAM** crystals, for instance, exhibit a peeling phenomenon[29,37], cis-**DVAM** crystals demonstrate autonomous behavior[38], including a P-type response of trans-**DVAM**[19], and trans-**AYAD** crystals are known for their photoinduced gel formation[39]. Crystals composed of trans-**ATF** possess a unique feature of light absorption, which leads to a temporary melting of the crystal structure, resulting in a collapse of the crystal matrix. This is then followed by a crystallization process, ultimately forming a mixed photoisomer mixture. The chemical structure of trans-**ATF** bears a striking resemblance to that of the previously examined anthracene derivatives. Remarkably, the alteration of the head-group connected to the di-olefin moiety (red color) induces a comprehensive shift in the photomechanical behavior of the molecule. In this preliminary report, we aim to introduce a novel molecule (trans-**ATF**) that exhibit three distinct features: 1) These materials have the ability to form star-shaped microcrystals (graphical abstract), reminiscent of the intricate structures found in sea anemones . 2) When exposed to visible

light, these crystals undergo fast photoinduced melting, temporarily transitioning into a liquid phase. 3) The photoinduced melted crystals revert back into their crystalline state spontaneously with the formation of a mixed photoisomer phase. The study encompasses a full synthesis and characterization of the derivative, including the provision of a CIF file containing its crystal structure. While the report offers a preliminary description of the photomechanical mechanism involved, it also includes several attached movies and SEM images, effectively illustrating the photomechanical phenomenon under investigation. The photomechanical engine operates through a trans-to-cis photoisomerization process involving the carbon-carbon double bond, as illustrated in **scheme-1**. The absorption spectra of the trans-**ATF** and cis-**ATF**, depicted in **Figure-1**, are generated by irradiating a solution of trans-**ATF** in acetonitrile using 532 nm light. This photochemical reaction, when induced in the crystalline state or in an aqueous suspension, results in a transient melting phenomenon followed by the re-crystallization of the mixed photoisomer phase.

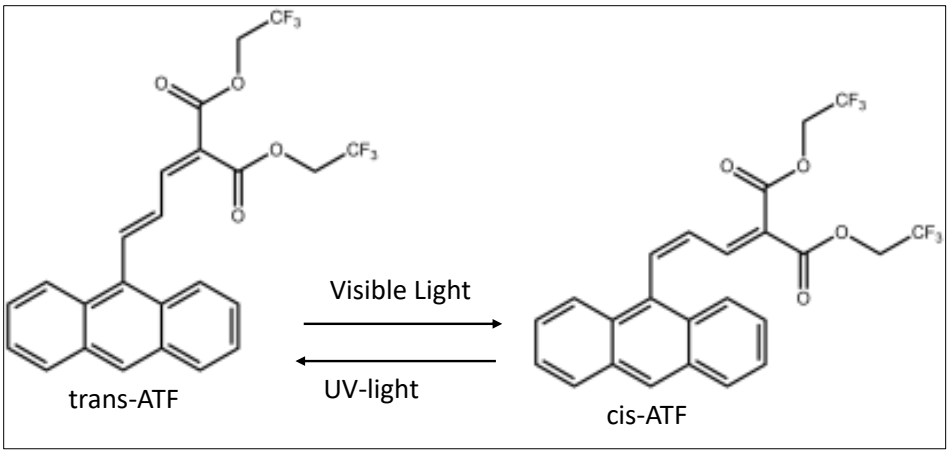

Scheme-1: Photoisomerization of Trans-ATF to cis-ATF

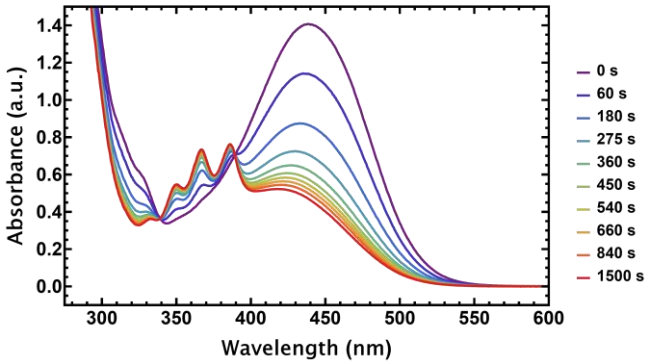

Figure-1: The absorption spectra of pure trans-ATF (violet @ 0 sec) and 92% pure cis-ATF (red @ 1500 sec) in acetonitrile using 532 nm laser light.

Surfactant-facilitated precipitation of hyperbranched crystals, formed from the trans-isomer coupled with photo-induced melting, exhibits behavior reminiscent of sea anemones. This unique structure can be harnessed to efficiently capture suspended particulates and entrap them within the crystalline phase.

Experimental

Part I: Synthesis

General: For the synthesis we utilized high-quality organic solvents, specifically reagent-grade solvents and spectroscopic-grade solvents, and were used without further purification. Thin layer chromatography (TLC) was performed on an aluminum backed silica gel GF254 plates measuring 5x2.5 cm. Detection of TLC spots was achieved through either UV light with a 254 nm wavelength or a chemical stain employing $KMnO_4$. The compound (E)-3-(anthracen-9-yl)acrylaldehyde 1 (>98%) was procured from TCI Tokyo and was used as received without further treatment. Malonic acid, 2,2,2-trifluoroethanol, pyridine, and piperidine were obtained from Sigma-Aldrich and were used in their original form. For Nuclear Magnetic Resonance (NMR) analysis, both 1H and 13C NMR spectra were recorded at 298 K on a JEOL spectrometer operating at 400 MHz. Proton chemical shifts were reported in parts per million (ppm) relative to DMSO-d6 as the reference at δ 2.50 ppm, and J values were reported in hertz (Hz). Carbon chemical shifts were also expressed in ppm (δ) using DMSO-d6 as the reference at δ 39.52 ppm. Full proton decoupling was applied during 13C NMR experiments. To improve solubility and prevent freezing, a 25% (v/v) mixture of DMSO-d6 in CCl4 was employed instead of pure DMSO-d6. Infrared (IR) measurements were conducted using an IR Affinity-1 FTIR instrument from Shimadzu. Approximately 1% of the sample was blended with spectroscopic grade KBr, and the resulting mixture was formed into a transparent pellet for analysis. High-Performance Liquid Chromatography (HPLC) was conducted using a Shimadzu LC-20AD system equipped with a Thermo Scientific general-purpose BDS Hypersil C18 column (250 × 4.6 mm dimensions). The column was maintained at a constant temperature of 35°C, and a gradient mobile phase was employed, starting with a mixture of 50% aqueous acetonitrile in water (pH = 2.5) and concluding with 100% acetonitrile, with a flow rate of 1.5 mL/min. The detector wavelength was set at 254 nm. UV analysis was carried out using a Spectro UV-Vis (UVD 2950) instrument from Labomed Inc., with a 1 cm quartz cell and a 1.0 nm slit width. The analysis was conducted within the wavelength range of 200-600 nm, with a solvent blank acquired before each measurement. Optical microscopy investigations were performed using an upright fluorescence microscope from Optika, equipped with a 100 W medium-pressure Hg lamp and a 2 MP digital camera. Various excitation wavelengths were attained through different optical filter combinations, and the typical irradiation intensity was approximately 10 mW/cm^2. Melting points (uncorrected) were determined using a 1101D Mel-Temp digital melting point apparatus.

For the synthesis of **trans-ATF** the following chemical reaction scheme-2 was adopted

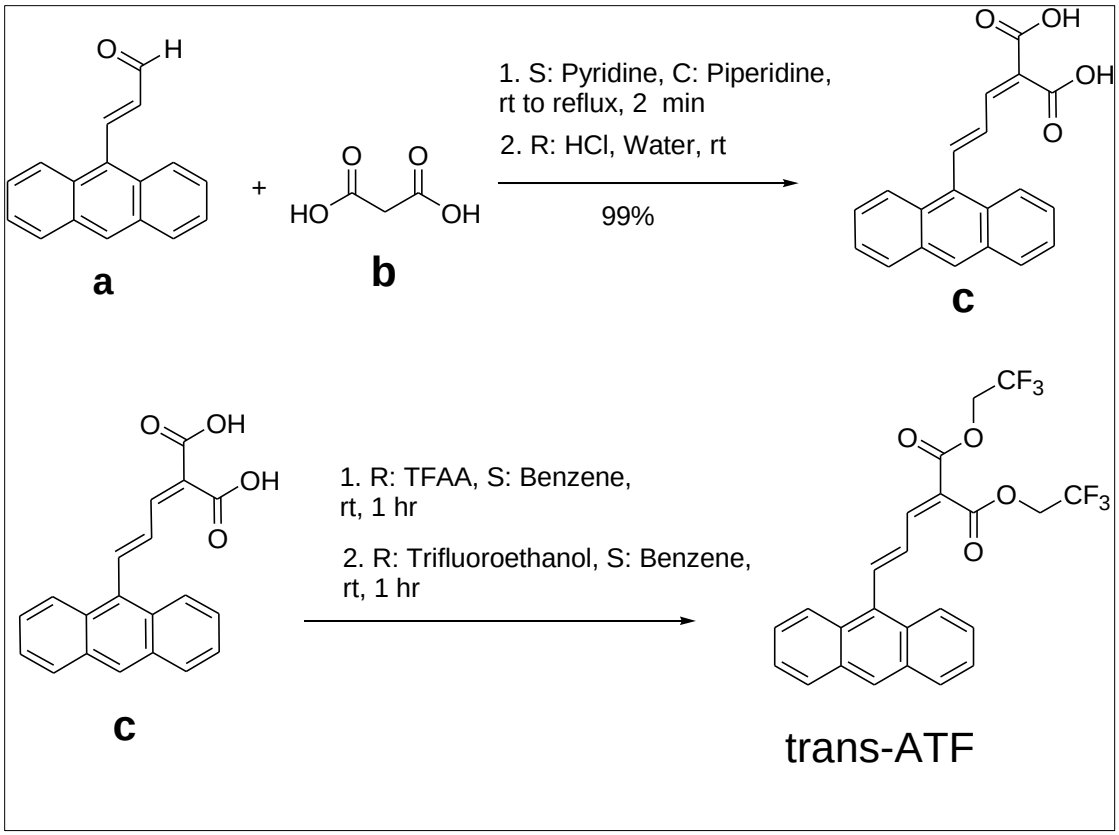

Scheme-2: A two-step Synthesis of **trans-ATF** from

1. Synthesis of 2-(3-Anthracen-9-yl-allylidene)-malonic acid (**c**): The synthesis process was carried out in a dark room with a 60 W red light. A 2.5 g (0.01 moles) solution of (E)-3-(anthracen-9-yl)acrylaldehyde (**a**) in pyridine (40 mL) was stirred at room temperature inside a 250 mL round-bottom flask, along with malonic acid (**b**) (5.2 g, 0.054 moles) and a catalytic amount of piperidine (0.2 mL) under an Argon gas blanket for 4 hours. The reaction progress was monitored by adding a few drops of the reaction mixture to water. The formation of a clear orange solution indicated the consumption of **a**. Subsequently, the reaction mixture was added to a mixture of concentrated HCl (400 mL) and 200 mL of crushed ice. The resulting precipitated diacid (**c**) was extracted with ethyl acetate (300 mL) and washed with water (2 x 100 mL). The organic layer was dried over anhydrous $MgSO_4$ and then gravity-filtered. The solvent was removed under reduced pressure at 40°C. Crude **c** was purified by sonicating with acetic acid (25 mL) and then precipitating the slurry with hexanes (200 mL). The fine red powder was collected by suction filtration and washed with hexane to remove excess acetic acid. The resulting product was air-dried, yielding 2.8 g of **c** red powder with an 82% yield and a melting point (dec.) of 205-206°C.

   1H NMR (400 MHz, DMSO-D6) δ 8.50 (s, 1H), 8.36 – 8.23 (m, 2H), 8.16 (d, J = 15.7 Hz, 1H), 8.04 (d, 2H), 7.83 (dd, J = 11.5, 0.8 Hz, 1H), 7.59 – 7.43 (m, 4H), 7.25 (dd, J = 15.7, 11.6 Hz, 1H). Figure-2

13C NMR (101 MHz, DMSO-D6) δ 166.34, 166.28, 143.75, 140.19, 132.63, 131.03, 130.46, 129.15, 128.67, 127.81, 126.28, 126.11, 125.16. Figure-3

The infrared (IR) spectrum of the product showed characteristic peaks: a broad peak in the range of 3300-2700 cm^{-1}, along with peaks at 1721, 1687, 1454, 1165, and 845 cm^{-1}.

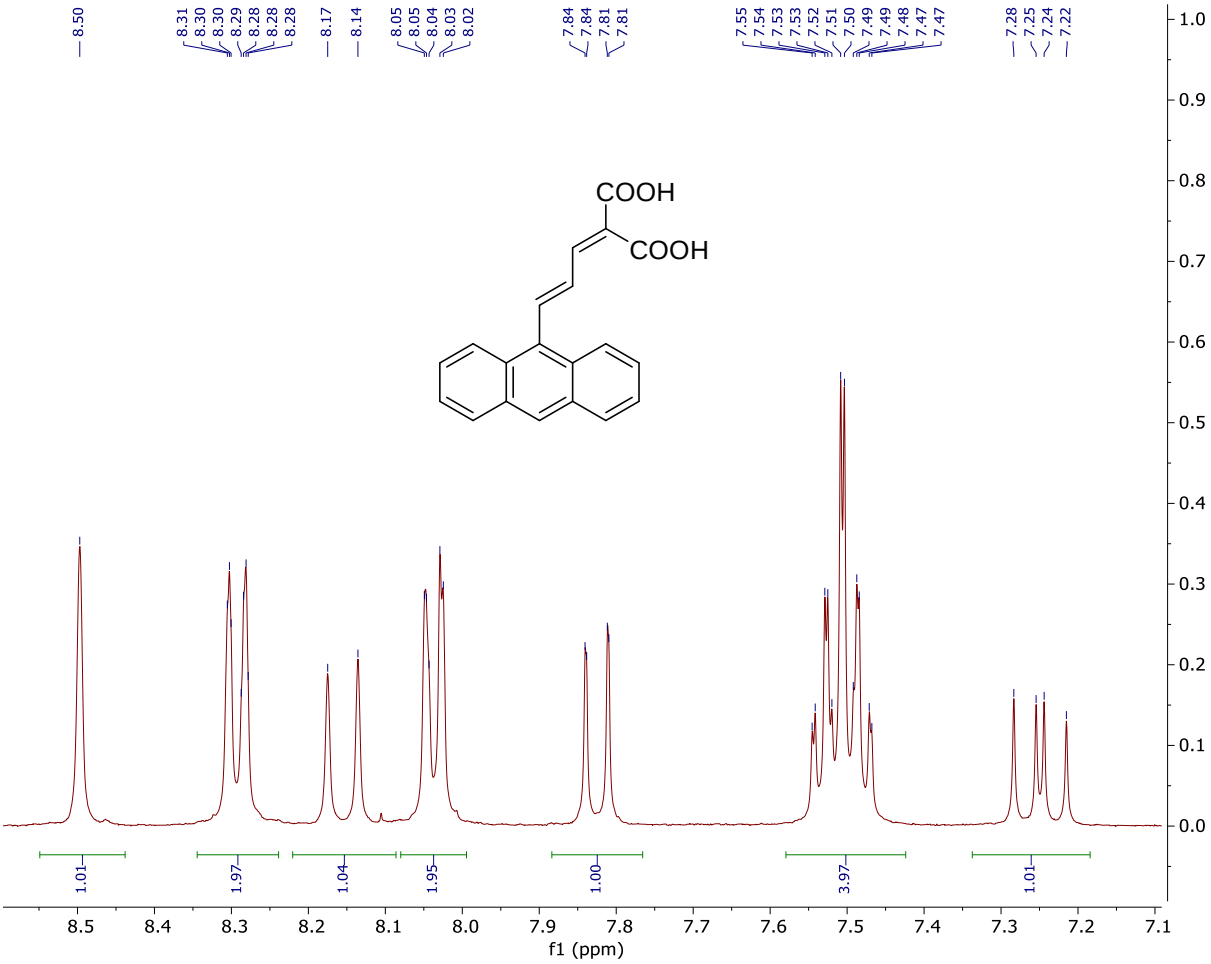

Figure-2: ^{1}H NMR of 2-(3-Anthracen-9-yl-allylidene)-malonic acid in 25% DMSO-d_6 in CCl_4

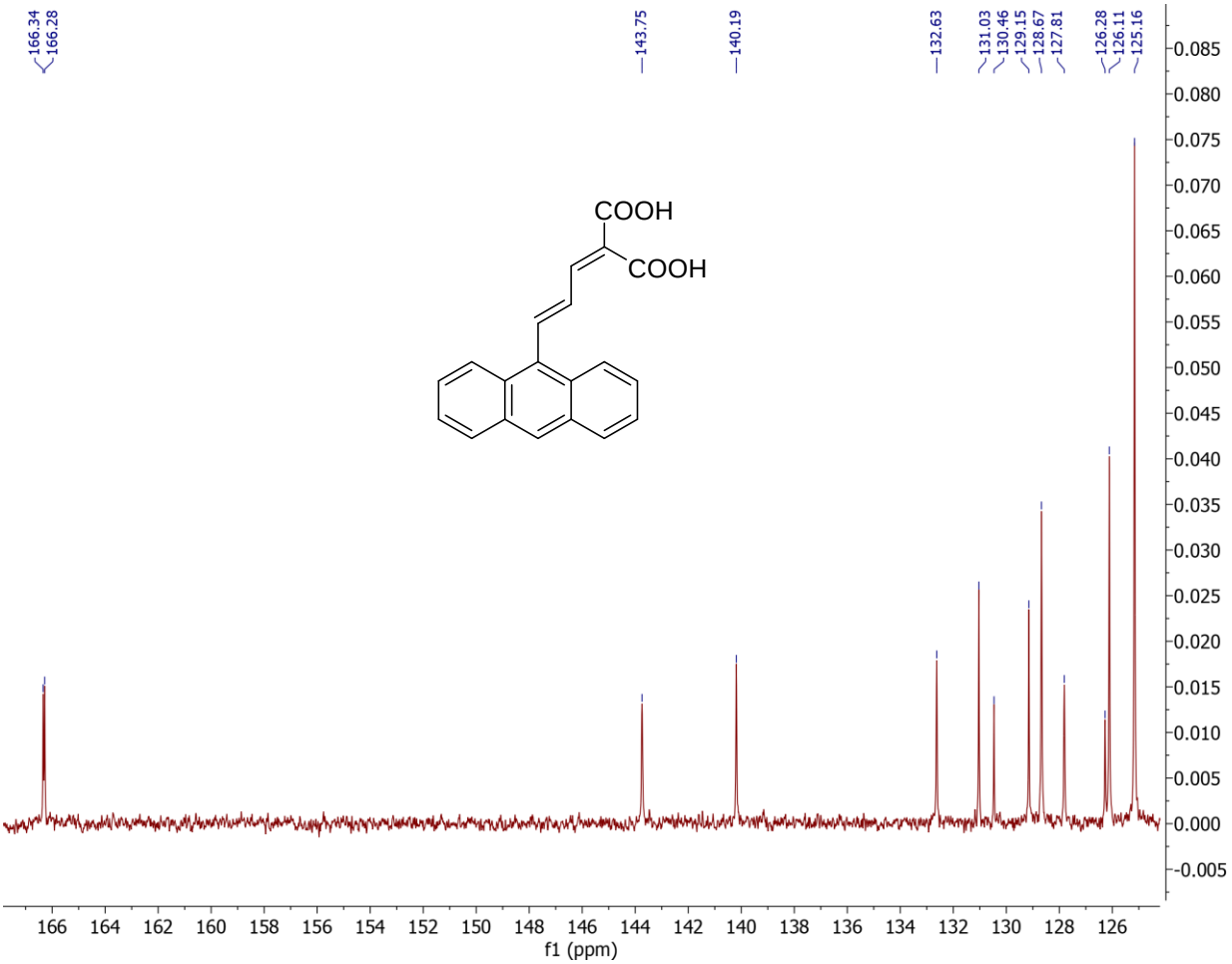

Figure-3: ^{13}C NMR of 2-(3-Anthracen-9-yl-allylidene)-malonic acid in 25% DMSO-d6 in CCl_4

2. Synthesis of **trans-ATF**: Into a flame-dried and Argon gas-purged 25 mL round bottom flask was added dry benzene (5 mL) via syringe. Derivative **c** (0.22 g) was added to the benzene to form a suspension. Trifluoroacetic anhydride (excess) was added via syringe to the stirring suspension of **c** and allowed to stir at room temperature under a blanket of Argon gas for 20-30 minutes or until the suspension went into solution. *2,2,2*-trifluoroethanol (excess) was added to the previous mixture and allowed to stir under Argon for 24 hours. Reaction progress was monitored using TLC (silica gel, Ethyl Acetate/ Hexane). The organic phase was washed with aqueous $NaHCO_3$ to remove the unreacted **c**, trifluoroacetic acid and alcohol and then dried over anhydrous $MgSO_4$. Additional 10 to 15 mL of dry benzene might be needed to compensate for the evaporated portions during workup. The organic phase was decanted and removed under reduced pressure to obtain crude product which was later recrystallized from minimum amount of boiling ethanol (10-15 mL) and water. Obtained light-yellow needles 0.17g (yield 60%) and a melting point of 93.5-95 °C

^1H NMR (400 MHz, DMSO-D_6) δ 8.53 (s, 1H), 8.48 (d, J = 15.5 Hz, 1H), 8.38 – 8.24 (m, 2H), 8.16 (d, J = 11.7 Hz, 1H), 8.05 (dd, J = 8.0, 1.9 Hz, 2H), 7.62 – 7.41 (m, 4H), 7.27 (dd, J = 15.5, 11.7 Hz, 1H), 4.82 (q, J = 8.6 Hz, 2H), 4.74 (q, J = 8.6 Hz, 2H). Figure-4

^{13}C NMR (101 MHz, DMSO-D_6) δ 162.55, 162.50, 149.73, 145.26, 131.56, 131.45, 130.10, 129.72, 129.19, 126.82, 125.65, 125.44, 121.19, 61.21, 60.74. Figure-5

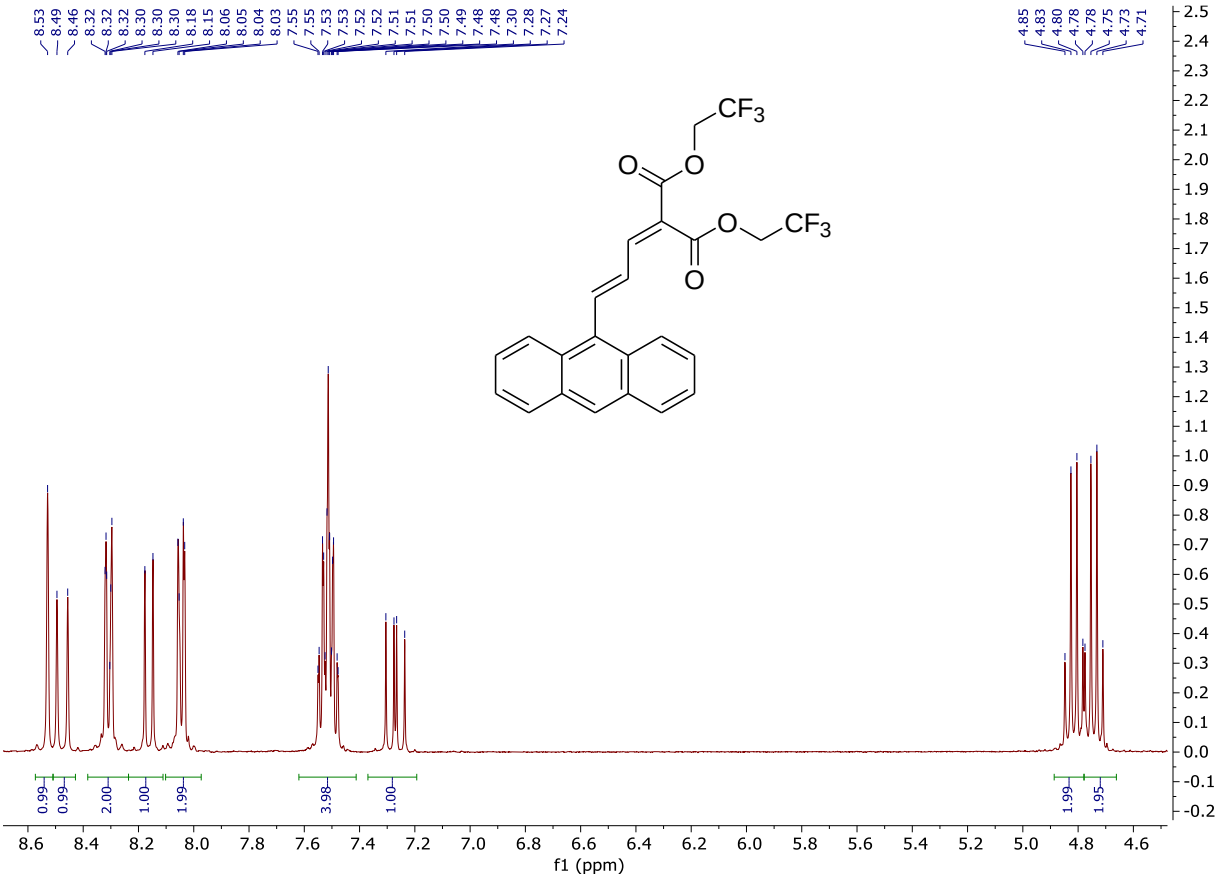

Figure-4: ^{1}H NMR of trans-ATF in 25% DMSO-d_6 in CCl_4

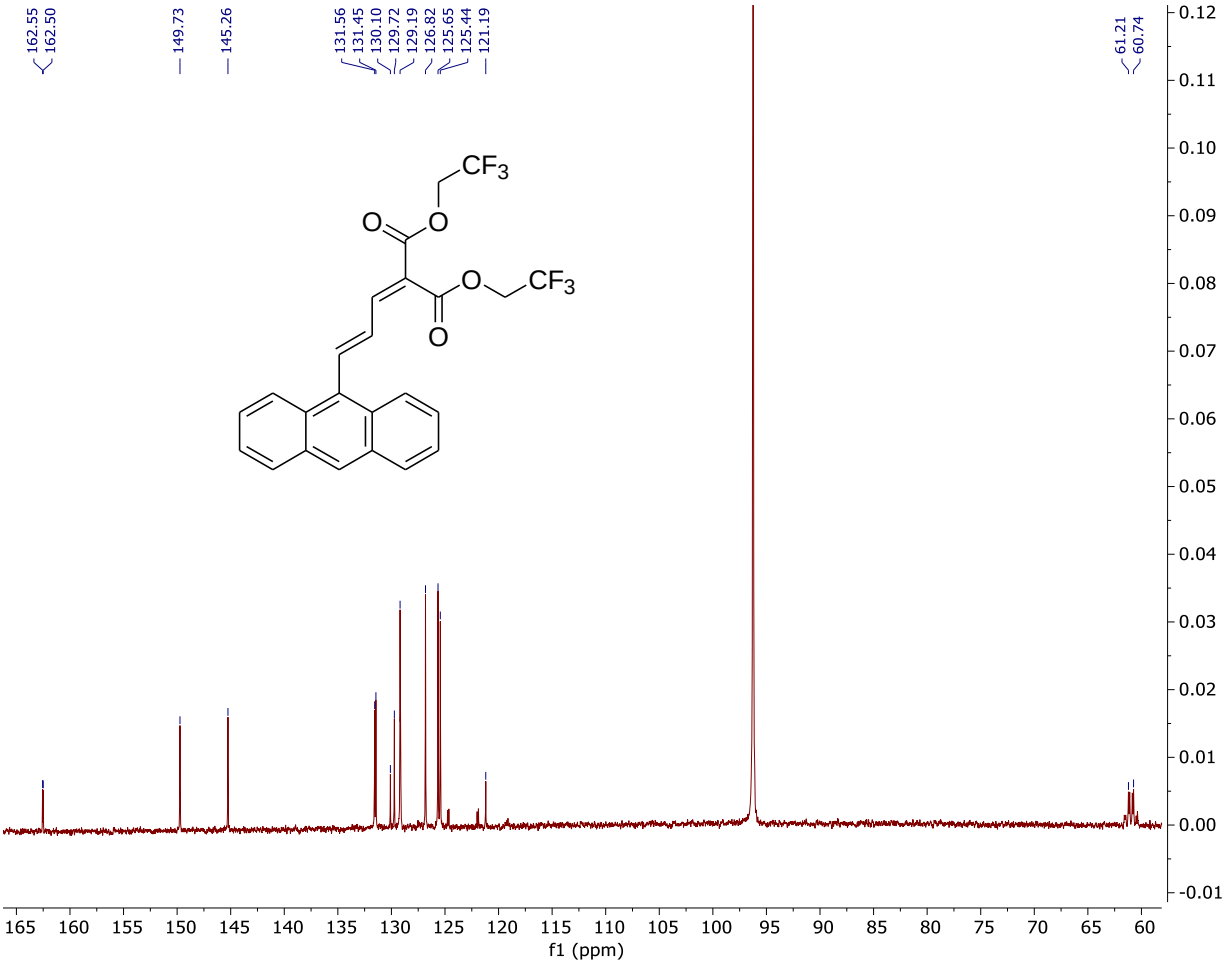

Figure-5: ^{13}C NMR of trans-ATF in 25% DMSO-d_6 in CCl_4

Photochemical Synthesis and Characterization of cis-ATF scheme-1:

Despite the efforts, achieving a 100% conversion of the trans-ATF to cis-ATF proved challenging due to the establishment of a photo-stationary state (Figure-1). However, through optimization, the photochemical conversion was successfully pushed to 93% cis-ATF, with a remaining 7% as trans-ATF. Further investigations into the factors influencing the photo-stationary state and the underlying kinetics of the reaction may offer insights for enhancing the conversion efficiency and understanding the photochemical behavior of ATF isomers.

In a 100 mL Schlenk flask, 50 mg of trans-ATF was dissolved in 50 mL of HPLC grade acetonitrile. The solution was then degassed with Argon to remove any dissolved oxygen and to create an inert atmosphere. Subsequently, the solution was irradiated with a 450 nm wavelength from a commercial Blue LED light strip. This light source is known to initiate the photoisomerization of trans-ATF to its cis-isomer. The reaction progress was monitored using High-Performance Liquid Chromatography (HPLC) to track the changes in the concentrations of cis-ATF and trans-ATF over time. The reaction was considered complete when the ratio of cis-ATF to trans-ATF became constant, indicating that the photoisomerization reached equilibrium. The HPLC analysis showed a conversion rate of 93% cis-ATF, which indicates a highly

efficient photoisomerization process. Finally, the solvent, acetonitrile, was removed under reduced pressure, leaving behind 50 mg of yellow crystals of cis-ATF with a melting point of 125-132°C. These crystals were found to be stable in the solid state, making them suitable for further characterization and use in various applications. A solution of the cis-ATF in acetonitrile was stable at room temperature with less than 5% reversion to the trans-ATF over a period of 24 hours.

1H NMR (400 MHz, DMSO-D6) δ 8.45 (s, 1H), 8.06 – 7.89 (m, 4H), 7.84 (d, J = 11.0 Hz, 1H), 7.53 – 7.30 (m, 5H), 7.12 (dd, J = 12.0, 0.9 Hz, 1H), 4.67 (q, J = 8.3 Hz, 2H), 4.30 (q, J = 8.2 Hz, 2H). Figure-6

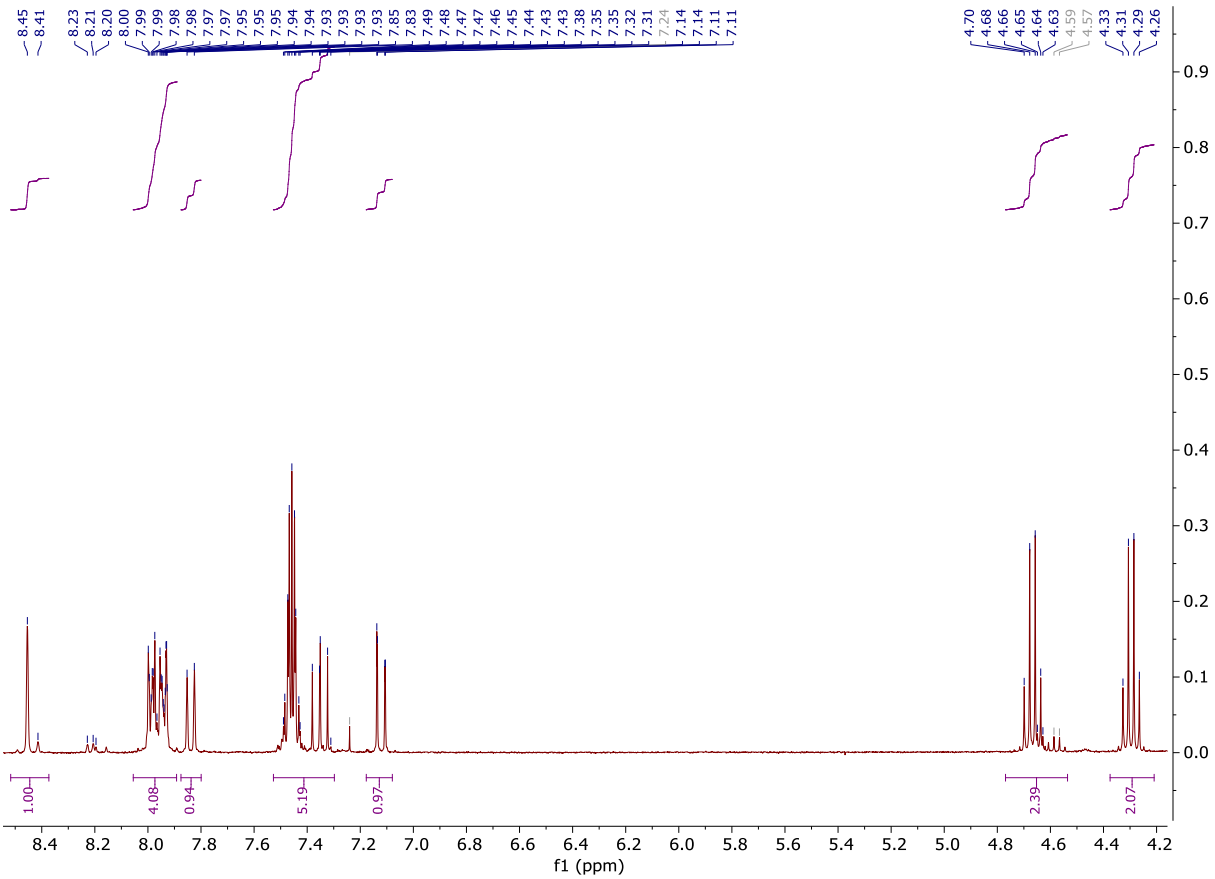

Figure-6: ^{1}H NMR of cis-ATF in 25% DMSO-d_6 in CCl_4

Part II: Fabrication and characterization of microwires and hyperbranched microcrystals.

In order to create uniform crystalline microstructures, we employed the seeded growth method using an aqueous surfactant[40]. The surfactant used in this study was a mixture of SDS (sodium dodecyl sulfate) and 1-DD (1-dodecanol) previously employed to grow uniform-shaped microcrystals form various organic compounds[29,41–43]. To initiate the process, we prepared a solution of trans-ATF in N,N-DMF (N,N-dimethylformamide) with a concentration of 1 mg ATF per 0.035 mL DMF. Subsequently, we prepared an aqueous solution containing 10 mL of SDS (0.025 M) mixed with 1-DD (0.0025 M), which was then warmed to 45°C. Into this mixture, we injected 50 microliters of the trans-ATF solution. This resulted in the formation of an oily suspension of ATF, which was incubated at 45°C for 24 hours. By subjecting the solution to slow annealing, we successfully achieved a uniform suspension of hyper-branched microcrystals. The resulting crystals were characterized using optical microscopy and SEM (scanning electron microscopy) techniques. Figure-7

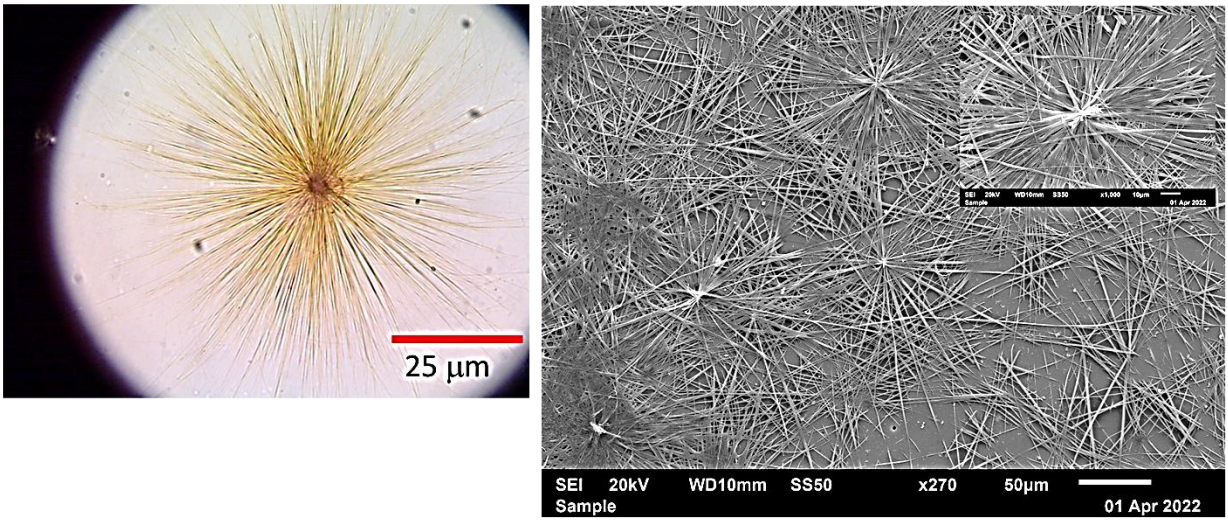

Figure-7: Hyperbranched trans-ATF microcrystals. Left image using optical microscopy. Right image, SEM of the microcrystals filtered through AAO template then air-dried and sputter coated with Pt.

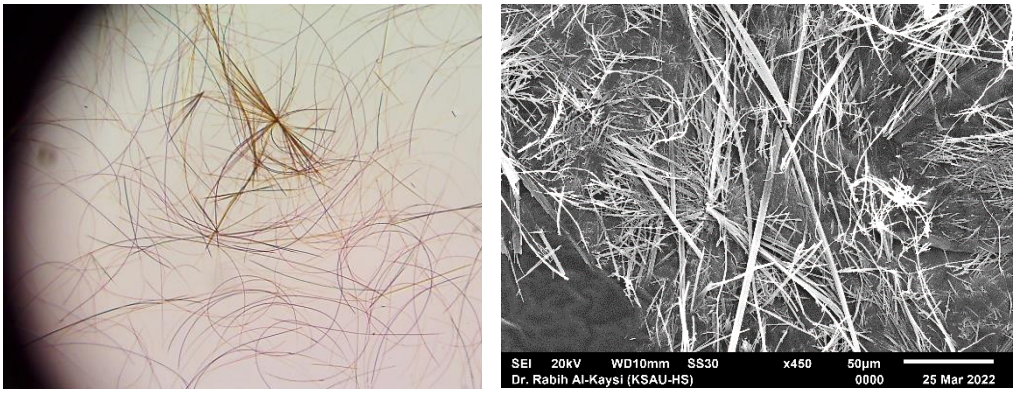

Figure-8: a) Optical microscope image of trans-ATF microwires suspended in aqueous media. B) SEM of the microwires over AAO template. The average thickness of the microwire is around 1 micron.

When the amount of injected ATF was reduced to 25 microliters and the oily suspension was slowly agitated using tumble rotation inside an oven set at 45 ^{o}C, a majority of isolated microwires were obtained instead of the hyperbranched crystals Figure-8. The formation of predominantly microwires proved to be reproducible across multiple batches. As long as the sample was gently agitated, the microwires were unable to aggregate and expand from a central hub.

The comprehensive characterization of the hyperbranched crystals was primarily based on optical microscopy images and scanning electron microscopy (SEM) of the samples. The SEM analysis involved a process in which the star-shaped crystal suspension was carefully filtered through an AAO (anodic aluminum oxide) template, followed by a gentle washing with deionized water (D.I. water). Subsequently, the sample was air-dried in a dark environment and then coated with a thin layer of Pt/Pd using sputter coating. This method allowed for a detailed examination of the hyperbranched crystals, enabling us to study their morphology and internal structure. Optical microscopy provided valuable information on the crystal's overall appearance and dimensions, while SEM offered higher resolution images, helping us observe finer surface features and obtain insight into their nanostructure.

Photomechanical studies:

As stated in the introduction, crystals composed of trans-ATF, when suspended in aqueous surfactant or water, exhibit the ability to absorb visible light and undergo a photochemical isomerization, converting to the cis-ATF isomer. However, it is noteworthy that unlike the efficient conversion observed in the solution of trans-ATF, the conversion process in the solid state is associated with the melting of the crystal phase, followed by subsequent crystallization. This solid-state photoconversion results in a lower yield of cis-isomer compared to the solution-phase conversion. HPLC and H-NMR analysis have verified that the composition of the solid-state photoconverted trans-ATF contains only 65% cis-ATF, with the remaining portion being unreacted trans-ATF. The a similar ratio of cis and trans ATF was obtained when the sample was irradiated with 475 nm light instead. **Figure-9**

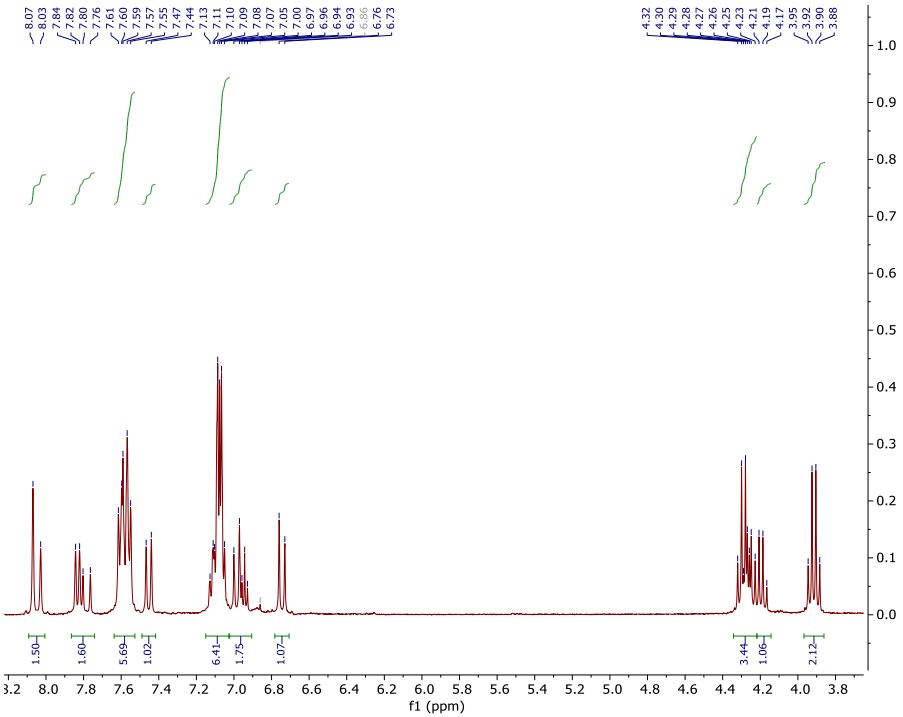

Figure-9: ^{1}H NMR of trans-ATF crystals after illumination with intense visible light. The H NMR contains a mixture of trans and cis-ATF

The intriguing behavior observed when trans-**ATF** crystals absorb visible light has motivated us to design crystals capable of harnessing this phenomenon in a functional manner. Under an optical microscope equipped with an intense light source from a medium pressure mercury lamp, directed through band-pass filters, we have observed a remarkable spontaneous melting phenomenon in trans-**ATF** crystals. This melting initiates at the edges of the crystal and progressively propagates towards the center, culminating in the spontaneous crystallization of a new photoisomer mixture. The movies included with this document are crucial for explaining the phenomenon. To enhance the reader's experience, we recommend downloading and viewing the movies for a more comprehensive understanding. A detailed description of each movie is included in the text. The movies are uploaded in the supplementary information section.

Movie-1: Initial observation of crystals of trans-ATF melting when exposed to visible light. A collection of large acicular crystalline fragments, immersed in an aqueous solution containing 0.025 molar SDS (sodium dodecyl sulfate) to aid in dispersing the crystals, exhibit an intriguing phenomenon. When exposed to broad-wavelength visible light from the microscope halogen lamp, these crystals undergo a remarkable process of melting and collapsing, eventually converging towards the central region. Initially, we notice a subtle photomechanical response from the crystals with slight bending a twisting followed by fast melting. The movie is in real-time. Frame width = 2.5 mm.

Movie-2: Utilizing a cross-polarized microscope, the macroscopic crystals featured in Movie-1 exhibit a characteristic birefringence indicative of crystalline organic substance. Upon subjecting the crystals to visible light, they undergo melting. This process unequivocally demonstrates the dissipation of birefringence, with the resultant mixed isomer ATF droplets adopting an amorphous configuration. After a brief duration, these droplets undergo spontaneous crystallization, accompanied by the revival of

birefringence within the newly formed crystalline phase. The ratio of trans to cis-ATF was retained in the new crystalline phase and was unchanged over time as revealed by H NMR analysis of the photolyzed sample. The isomeric ratio does not change even after prolonged light exposure, thus attaining a photostationary state. The movie is in real-time and the frame width = 0.25 mm

The experiments portrayed in Movies-1 and 2 validate the following observations:

1. The trans-ATF commences in a crystalline state during its initial phase.
2. Upon exposure to moderately intense visible light or 475 nm light, selectively filtered through a band pass filter, the crystalline structures undergo a transformation induced by a trans to cis photochemical reaction. This transformation leads to the melting and disintegration of the crystals, resulting in the formation of suspended oily droplets.
3. Following this, the suspended oily droplets undergo a photochemical equilibrium, with ATF molecules adopting a 65% cis and 35% trans configuration. This equilibrium subsequently initiates the recrystallization process of these droplets, transforming them back into spherical crystalline structures.

These experimental findings shed light on the intricate interplay between light-induced changes in molecular conformation and the resulting macroscopic transformations, highlighting the dynamic behavior of the trans-ATF system.

The preliminary investigation of the photomelting process revolved around an examination of bulk crystals of trans-ATF. In order to harness the potential of the photoinduced melting phenomenon effectively, it became apparent that shaping these crystals into precise and well-defined geometrical configurations was advantageous. Given the constraints inherent in the molecular structure of trans-ATF and the natural tendencies of crystal formation, an engineered structure, achieved through the surfactant-seeded growth method, took the form of uniform and slender microwires. In a real-time observational scenario, a captivating sequence was recorded, wherein suspended microwires were subjected to irradiation with 475 nm light with intensity that can be modulated using neutral density filters. In the course of this irradiation, the microwires exhibited subtle undulating motions before eventually succumbing to spontaneous melting. This melting process was characterized by a progressive collapse of the microwire tip that simultaneously emanated from both termini of the microwire. The observed phenomenon bears resemblance to the propagation of combustion in a fuse, wherein the photomelting progression advances uniformly throughout the length of the microwire.

Movie-3: Microwires of trans-ATF, sharing comparable dimensions in terms of thickness (averaging 2 microns), were grown through the seeded growth technique from aqueous surfactant. These microwires were suspended in an aqueous solution of SDS (sodium dodecyl sulfate). Upon irradiation with 475 nm light (or visible light), a sequence of events unfolded. Initially, the microwires exhibited subtle oscillatory movements, suggestive of a photomechanical response to the light stimulus. This prelude was succeeded by spontaneous melting commencing at the extremities of the microwires. This anisotropic melting progression extended longitudinally towards the center of the wire, originating concurrently from both terminal points. This dynamic transformation culminated in the generation of suspended droplets, characterized by a molten state. Subsequently, this molten state underwent crystallization, effectively solidifying the droplets within the surrounding medium. The chemical composition of the

droplets mirrors the composition of cis and trans-ATF obtained from the acicular crystals from movies-1 and 2. The key benefit of employing consistently shaped microwires made from trans-ATF is the ability to induce photo-melting uniformly across the entire sample. The rate of photomelting can be increased by increasing the intensity of visible light or 475 nm light used. In addition, photomelting can be stopped midway before the entire wire collapses into a liquid droplet by simply reducing the light intensity. The movie is in real-time and the frame width = 1 mm.

Through manipulation of the initial conditions inherent to the seeded growth methodology, it becomes possible to initiate the formation of hyperbranched microcrystalline architectures. These hyperbranched microcrystalline entities exhibit a nearly uniform morphology, characterized by an average diameter measuring 100-50 microns. These structures contain micro-crystalline projections radiating outward from a central hub reminiscent of sea anemones. Upon suspension in an aqueous SDS medium, the hyperbranched microcrystals induce a perceptible opaqueness within the liquid medium. However, when exposed to intense visible light, a notable transformation takes place. The solution undergoes a transition from opacity to heightened transparency, a change attributed to the collapse of the intricate crystalline arrangement. This collapse leads to the formation of suspended droplets and an enhanced clarity of the solution.

Movie-4, 5, 6: Upon exposure to visible light, a branched microcrystal composed of trans-ATF undergoes a rapid photoinduced melting process. This leads to a pronounced structural collapse, wherein the various branches converge towards the central axis, resulting in a substantial reduction in overall dimensions. Following this dynamic transformation, the resultant liquid droplet gradually crystallizes. This crystallization is manifest through the emergence of distinct facets along the droplet's periphery, indicative of the crystalline lattice's formation. **movie-5, 6** : Similar to **movie-4**. The movies are in real-time and the frame width for **Movie-4, 5** = 0.25 mm, **Movie-6** = 0.1 mm.

The anisotropic melting characteristics exhibited by star-shaped trans-ATF crystals result in the formation of liquid droplets at the extremities of each melting appendage. These droplets function as adhesive hooks during their progression toward the crystal's central region. These adhesive droplets may be harnessed to adhere to suspended particulate matter in the proximity of the branched crystal and subsequently transport them towards the center of the melting crystal. As a proof-of-concept, we conducted an experiment where we suspended silica microparticles and clusters within star-shaped crystals, subjecting them to intense illumination. When exposed to high-intensity light, the melting process occurred rapidly, leaving little time for the crystalline branches to capture and draw the suspended particles towards the center. This phenomenon is clearly observable in both **Movie-7** (frame width = 0.2 mm) and **Movie-8** (frame width = 0.2 mm), both of which were recorded in real-time using unattenuated 475 nm light. The collapse of the branched crystals outpaced the ability of their arms to grasp the suspended silica debris and pull it towards the center. However, by reducing the intensity of the 475 nm light source, we observed that the crystalline branches melted more slowly, allowing them sufficient time to engage with some of the suspended debris and gradually pull it towards the center.

Movie-9, 10 ,11: When the light source is attenuated using neutral density filters, the hyperbranched structure begins to melt from the tentacles increasing the stickiness of these tentacles that grab silica microspheres towards the center of the microstructure. The photo-melted phase traps inside the microparticles then crystallizes. Although we lack direct evidence of the presence of silica microspheres

trapped inside the matrix. Similar behavior is depicted in **movie-10** and **movie-11**. All movies are in real-time and frame width = 0.2 mm

Discussion:

The phenomenon of photoinduced melting in molecular crystals is predominantly observed in certain azobenzene derivatives[33]. Some of these compounds can transition from a solid to a liquid phase upon exposure to specific wavelengths of light due to the formation of a photoisomer that disrupts the crystal packing of the reacting molecule. Photothermal effects have been excluded in many cases, as the liquid state can be solidified by irradiation with an appropriate wavelength to regenerate the trans isomer. Numerous instances of photoinduced solid-to-liquid transitions have been documented in the scientific literature. For instance, when crystals of certain azobenzene derivatives are exposed to the appropriate wavelength of light, photoisomerization takes place, resulting in the formation of a predominant isomer. The outcome of this phase transition is heavily influenced by the specific azobenzene derivative under investigation. In some cases, it has been observed that irradiation of a liquid sample with a different wavelength of light can reverse the melted photoisomeric mixture back to its solid state. This reversible phase transition underscores the sensitivity of these molecular crystals to external stimuli. In particularly noteworthy cases, researchers have employed dual-wavelength irradiation, strategically angled relative to the azobenzene derivative, to induce a controlled and gradual melting and solidification process[36]. This unique manipulation allows the crystal to slowly traverse along a glass slide, highlighting the precision and versatility of the photoinduced melting phenomenon. Photoinduced crystal-to-liquid transition has also been observed in trans-to-cis photoisomerization in olefin-containing derivatives. An illustrative example pertains to divinyl-naphthalene crystals, specifically dimethyl (E)-2-(3-(naphthalen-1-yl)allylidene)malonate, which can transition to a liquid state upon absorbing ultraviolet (UV) light. This transformation results in a liquid mixture containing both E and Z isomers, which remains in a liquid state indefinitely. However, the rate of this transformation is significantly slower compared to the system discussed in this article[44]. Another example involves the E-to-Z photoinduced crystal-to-liquid transformation of an acylhydrazone derivative of methoxy naphthalene[45]. What distinguishes this system and underscores its advantages in current research is the simplicity of the required stimulus. Visible light is sufficient to initiate the rapid transition of these crystals from a crystal to a liquid state followed by spontaneous crystallization. This inherent property simplifies the experimental setup and holds promise for diverse applications across various scientific and technological domains.

To mitigate the potential occurrence of a photothermal effect resulting in crystal melting, instead of achieving the intended photoinduced isomerization and disruption of the crystal matrix, we conducted measurements on the melting points of both the trans and cis forms of ATF. The obtained melting points significantly exceeded the ambient temperature, with the cis-ATF displaying a melting point approximately 30 degrees higher than that of the trans-ATF (for detailed experimental information, please refer to the experimental section). The solid-state photolysis mixture comprised of 65% cis-ATF and 35% trans-ATF exhibited a broad melting point (softens at 105°C), which remained notably higher than the melting point of pure trans-ATF. Furthermore, the occurrence of photoinduced melting in thin nanowires suspended in aqueous solution dismisses the possibility of a photothermal effect. This is due to water's efficient heat-dissipating properties, which should prevent the nanowires from reaching elevated temperatures and buildup of thermal energy to trigger melting. Additional evidence refuting

thermal-induced melting is the distinct anisotropic melting observed at the edges of the microwire or branched crystals, as opposed to a uniform, isotropic melting process.

The unique properties of the trifluoroethyl group in inducing photoinduced melting in **trans-ATF** were further clarified through the synthesis of an analog derivative of **trans-ATF**. In this derivative, two ethyl ester groups **trans-DMAE** replaced the trifluoroethyl esters. Importantly, the absorption spectrum of this

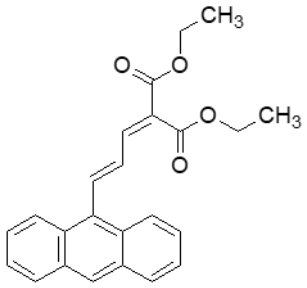

trans-DMAE

derivative closely matches that of **trans-ATF**. When we grew crystals using a surfactant-mediated seeded growth method with **trans-DMAE**, they displayed light absorption/ emission behavior without undergoing melting or exhibiting any photomechanical responses. This outcome aligns with our expectations, as it is well-established that the molecular arrangement within a crystal can significantly influence its photomechanical properties. This result underscores that the observed photoinduced melting phenomenon in **trans-ATF** cannot be attributed to photothermal effects. Instead, it appears to be a finely balanced interplay between the rate of formation of **cis-ATF** and the gradual crystallization of the photoisomer mixture. This delay, lasting approximately one minute, is sufficient to transform the hyperbranched crystal structure into a liquid state, followed by subsequent crystallization. In cases where the light intensity was reduced 1/32 the using ND32 , the star-shaped microcrystals melt at a slower rate, however the rate of photoinduced melting matches with the rate of crystallization leading to a semi collapsed microcrystal structure as depicted in **movie-12**. Additionally, we encountered inadvertent instances where **trans-ATF** polymorphs grew into sizable microsheets. While we did not fully elucidate the crystal structure of these polymorphs, subjecting them to similar light frequencies and intensities did not induce melting, and they remained unresponsive to the light stimulus Figure-10, **movie-13**. This provides further compelling evidence against photothermal effects being the only driving force behind the observed phenomena.

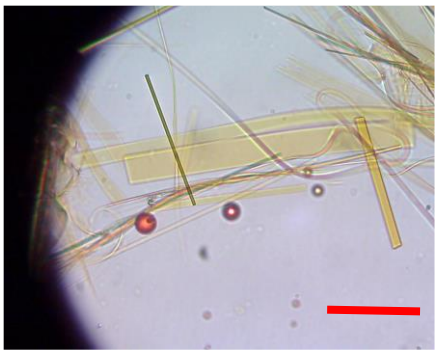

Figure-10: Optical microscope image of intact trans-ATF microcrystal sheets polymorph and melted trans-ATF crystals (orange droplets) after exposure to visible light. Scale bar = 25 μm

It's noteworthy that the photoisomerization induced melting of trans-ATF is not contingent on the surrounding medium. Even in the absence of an aqueous surfactant, dry crystals exhibit this phenomenon. Additionally, an intriguing observation is the reluctance of small submicron diameter liquid droplets resulting from the photomelting of trans-ATF to spontaneously crystallize. This size-dependent crystallization behavior is akin to the behavior of ultra small liquid water droplets that resist freezing due to the dominance of surface tension, which hinders crystal formation.

A potential explanation for the phenomenon of transient photoinduced melting can be linked to the presence of crystal defects located at the tip of the trans-ATF microwires. This phenomenon becomes evident when we observe **Movie-3** and the subsequent movies in our study. It is observed that the melting initiates at the edge of the microwire, where the trans-ATF is free to undergo photoconversion into **cis-ATF**. This specific process could potentially trigger a cascade of disruptions within the **trans-ATF** crystal lattice, resulting in the formation of a pseudo-eutectic mixture of photoisomers. The rate of photoconversion from trans to cis is faster than the rate of crystallization, which ultimately leads to the transient melted state that we have observed. We do not rule out that photoinduced melting occurs on the surface of the microwire, however, we believe that the rate is slower..

Conclusion:

In our pursuit of expanding the library of photomechanical molecular crystals, we have successfully synthesized the anthracene derivative **trans-ATF**. This compound exhibits the unique ability to form microcrystals characterized by distinct shapes and morphologies. We employ a seeded growth precipitation method utilizing an aqueous surfactant for the controlled growth of these microcrystals. Notably, the resultant microcrystals assume a star-shaped morphology resembling sea Urchins, and they possess a remarkable property: they can be undergo photomelting when exposed to visible light. This photoinduced anisotropic transformation from a crystalline state to a liquid phase initiates at the periphery of the star-shaped crystals and progressively proceeds towards the center, ultimately resulting in the complete melting of the microcrystal. Subsequently, a transient molten state composed of an isomeric mixture of cis and trans-ATF is formed. Over a brief period, this molten phase spontaneously recrystallizes. This unique interplay of photoinitiated melting followed by spontaneous crystallization presents an intriguing opportunity. Specifically, it can be leveraged for the capture and immobilization of suspended silica microparticles.

Acknowledgments: The authors like to acknowledge the continued support of the college of science and health professions at KSAU-HS and the KAIMRC at the Ministry of National Guard Health Affairs.

Conflicts of Interest: The authors declare no conflict of interest

References:

(1) Awad, W. M.; Davies, D. W.; Kitagawa, D.; Mahmoud Halabi, J.; Al-Handawi, M. B.; Tahir, I.; Tong,

F.; Campillo-Alvarado, G.; Shtukenberg, A. G.; Alkhidir, T.; Hagiwara, Y.; Almehairbi, M.; Lan, L.; Hasebe, S.; Karothu, D. P.; Mohamed, S.; Koshima, H.; Kobatake, S.; Diao, Y.; Chandrasekar, R.; Zhang, H.; Sun, C. C.; Bardeen, C.; Al-Kaysi, R. O.; Kahr, B.; Naumov, P. Mechanical Properties and Peculiarities of Molecular Crystals. *Chemical Society Reviews*. Royal Society of Chemistry April 18, 2023, pp 3098–3169. https://doi.org/10.1039/d2cs00481j.

(2) Naumov, P.; Chizhik, S.; Panda, M. K.; Nath, N. K.; Boldyreva, E. Mechanically Responsive Molecular Crystals. *Chem. Rev.* **2015**, *115* (22), 12440–12490. https://doi.org/10.1021/acs.chemrev.5b00398.

(3) Kim, T.; Zhu, L.; Al-Kaysi, R. O.; Bardeen, C. J. Organic Photomechanical Materials. *ChemPhysChem* **2014**, *15* (3), 400–414. https://doi.org/10.1002/cphc.201300906.

(4) Kobatake, S.; Takami, S.; Muto, H.; Ishikawa, T.; Irie, M. Rapid and Reversible Shape Changes of Molecular Crystals on Photoirradiation. *Nature* **2007**, *446* (7137), 778–781. https://doi.org/10.1038/nature05669.

(5) Al-Kaysi, R. O.; Müller, A. M.; Bardeen, C. J. Photochemically Driven Shape Changes of Crystalline Organic Nanorods. *J. Am. Chem. Soc.* **2006**, *128* (50), 15938–15939. https://doi.org/10.1021/ja064535p.

(6) Al-Kaysi, R. O.; Bourdelande, J. L.; Gallardo, I.; Guirado, G.; Hernando, J. Investigation of an Acid-Base and Redox Molecular Switch: From Bulk to the Single-Molecule Level. *Chem. - A Eur. J.* **2007**, *13* (25), 7066–7074. https://doi.org/10.1002/chem.200700236.

(7) Taniguchi, T.; Asahi, T.; Koshima, H. Photomechanical Azobenzene Crystals. *Crystals* **2019**, *9* (9), 437. https://doi.org/10.3390/cryst9090437.

(8) Koshima, H.; Taniguchi, T.; Asahi, T. Mechanically Responsive Crystals by Light and Heat. In *Mechanically Responsive Materials for Soft Robotics*; Wiley-VCH Verlag GmbH & Co. KGaA, 2019; pp 57–82. https://doi.org/10.1002/9783527822201.ch3.

(9) Koshima, H. *Mechanically Responsive Materials for Soft Robotics*; Koshima, H., Ed.; Wiley: New York, 2019. https://doi.org/10.1002/9783527822201.

(10) Naumov, P.; Chizhik, S.; Commins, P.; Boldyreva, E. Bending, Jumping, and Self-Healing Crystals. In *Mechanically Responsive Materials for Soft Robotics*; Wiley-VCH Verlag GmbH & Co. KGaA, 2019; pp 105–138. https://doi.org/10.1002/9783527822201.ch5.

(11) Abendroth, J. M.; Bushuyev, O. S.; Weiss, P. S.; Barrett, C. J. Controlling Motion at the Nanoscale: Rise of the Molecular Machines. *ACS Nano* **2015**, *9* (8), 7746–7768. https://doi.org/10.1021/acsnano.5b03367.

(12) Yadava, K.; Vittal, J. J. Solid-State Photochemical [2+2] Cycloaddition Reaction of MnII Complexes. *Chem. - A Eur. J.* **2019**, *25* (44), 10394–10399. https://doi.org/10.1002/chem.201901237.

(13) Tong, F.; Xu, W.; Guo, T.; Lui, B. F.; Hayward, R. C.; Palffy-Muhoray, P.; Al-Kaysi, R. O.; Bardeen, C. J. Photomechanical Molecular Crystals and Nanowire Assemblies Based on the [2+2] Photodimerization of a Phenylbutadiene Derivative. *J. Mater. Chem. C* **2020**, *8* (15), 5036–5044. https://doi.org/10.1039/c9tc06946a.

(14) Zhou, B.; Yan, D. Recent Advances of Dynamic Molecular Crystals with Light-Triggered Macro-Movements. *Appl. Phys. Rev.* **2021**, *8* (4), 041310. https://doi.org/10.1063/5.0059919.

(15) Bhandary, S.; Beliš, M.; Kaczmarek, A. M.; Van Hecke, K. Photomechanical Motions in Organoboron-Based Phosphorescent Molecular Crystals Driven by a Crystal-State [2 + 2] Cycloaddition Reaction. *J. Am. Chem. Soc.* **2022**, *144* (48), 22051–22058. https://doi.org/10.1021/jacs.2c09285.

(16) Zhu, L.; Agarwal, A.; Lai, J.; Al-Kaysi, R. O.; Tham, F. S.; Ghaddar, T.; Mueller, L.; Bardeen, C. J. Solid-State Photochemical and Photomechanical Properties of Molecular Crystal Nanorods Composed of Anthracene Ester Derivatives. *J. Mater. Chem.* **2011**, *21* (17), 6258–6268. https://doi.org/10.1039/c1jm10228a.

(17) Chalek, K. R.; Dong, X.; Tong, F.; Kudla, R. A.; Zhu, L.; Gill, A. D.; Xu, W.; Yang, C.; Hartman, J. D.; Magalhães, A.; Al-Kaysi, R. O.; Hayward, R. C.; Hooley, R. J.; Beran, G. J. O.; Bardeen, C. J.; Mueller, L. J. Bridging Photochemistry and Photomechanics with NMR Crystallography: The Molecular Basis for the Macroscopic Expansion of an Anthracene Ester Nanorod. *Chem. Sci.* **2021**, *12* (1), 453–463. https://doi.org/10.1039/d0sc05118g.

(18) Zhu, L.; Tong, F.; Salinas, C.; Al-Muhanna, M. K.; Tham, F. S.; Kisailus, D.; Al-Kaysi, R. O.; Bardeen, C. J. Improved Solid-State Photomechanical Materials by Fluorine Substitution of 9-Anthracene Carboxylic Acid. *Chem. Mater.* **2014**, *26* (20), 6007–6015. https://doi.org/10.1021/cm502866e.

(19) Zhu, L.; Tong, F.; Zaghloul, N.; Baz, O.; Bardeen, C. J.; Al-Kaysi, R. O. Characterization of a P-Type Photomechanical Molecular Crystal Based on the: E → Z Photoisomerization of 9-Divinylanthracene Malonitrile. *J. Mater. Chem. C* **2016**, *4* (35), 8245–8252. https://doi.org/10.1039/c6tc02517j.

(20) Zhu, L.; Al-Kaysi, R. O.; Bardeen, C. J. Photoinduced Ratchet-Like Rotational Motion of Branched Molecular Crystals. *Angew. Chemie - Int. Ed.* **2016**, *55* (25), 7073–7076. https://doi.org/10.1002/anie.201511444.

(21) Tong, F.; Kitagawa, D.; Dong, X.; Kobatake, S.; Bardeen, C. J. Photomechanical Motion of Diarylethene Molecular Crystal Nanowires. *Nanoscale* **2018**, *10* (7), 3393–3398. https://doi.org/10.1039/c7nr09571f.

(22) Kitagawa, D.; Tanaka, R.; Kobatake, S. Photoinduced Stepwise Bending Behavior of Photochromic Diarylethene Crystals. *CrystEngComm* **2016**, *18* (38), 7236–7240. https://doi.org/10.1039/c6ce00607h.

(23) Kitagawa, D.; Kobatake, S. Crystal Thickness Dependence of Photoinduced Crystal Bending of 1,2-Bis(2-Methyl-5-(4-(1-Naphthoyloxymethyl)Phenyl)-3-Thienyl) Perfluorocyclopentene. *J. Phys. Chem. C* **2013**, *117* (40), 20887–20892. https://doi.org/10.1021/jp4083079.

(24) Hirano, A.; Kitagawa, D.; Kobatake, S. Photomechanical Bending Behavior of Photochromic Diarylethene Crystals Induced under Polarized Light. *CrystEngComm* **2019**, *21* (15), 2495–2501. https://doi.org/10.1039/C9CE00175A.

(25) Kitagawa, D.; Bardeen, C. J.; Kobatake, S. Symmetry Breaking and Photomechanical Behavior of Photochromic Organic Crystals. *Symmetry (Basel).* **2020**, *12* (9), 1478. https://doi.org/10.3390/sym12091478.

(26) Kim, T.; Al-Kaysi, R. O.; Bardeen, C. J. Molecular Crystal Nanostructures That Undergo Reversible Photo-Induced Bending, Twisting, and Curling. In *Materials Research Society*; 2013.

(27) Huang, C.; Huang, R.; Zhang, S.; Sun, H.; Wang, H.; Du, B.; Xiao, Y.; Yu, T.; Huang, W. Recent

Development of Photodeformable Crystals: From Materials to Mechanisms. *Research* **2021**, *2021*, 1–26. https://doi.org/10.34133/2021/9816535.

(28) Kim, T.; Al-Muhanna, M. K.; Al-Suwaidan, S. D.; Al-Kaysi, R. O.; Bardeen, C. J. Photoinduced Curling of Organic Molecular Crystal Nanowires. *Angew. Chemie - Int. Ed.* **2013**, *52* (27), 6889–6893. https://doi.org/10.1002/anie.201302323.

(29) Tong, F.; Al-Haidar, M.; Zhu, L.; Al-Kaysi, R. O.; Bardeen, C. J. Photoinduced Peeling of Molecular Crystals. *Chem. Commun.* **2019**, *55* (26), 3709–3712. https://doi.org/10.1039/c8cc10051a.

(30) Nakagawa, Y.; Morimoto, M.; Yokojima, S.; Nakamura, S.; Uchida, K. Efficient Surface Peeling, a Photoinduced Result of Photochromic Diarylethene Crystal by Multistep Light Irradiation. *Cryst. Growth Des.* **2023**, *23* (3), 1581–1591. https://doi.org/10.1021/acs.cgd.2c01202.

(31) Tamaoki, M.; Kitagawa, D.; Kobatake, S. Light-Driven Rapid Peeling of Photochromic Diarylethene Single Crystals. *Cryst. Growth Des.* **2021**, *21* (5), 3093–3099. https://doi.org/10.1021/acs.cgd.1c00270.

(32) Balzani, V.; Credi, A.; Venturi, M. Light Powered Molecular Machines. *Chem. Soc. Rev.* **2009**, *38* (6), 1542–1550. https://doi.org/10.1039/b806328c.

(33) Xu, W. C.; Sun, S.; Wu, S. Photoinduced Reversible Solid-to-Liquid Transitions for Photoswitchable Materials. *Angew. Chemie - Int. Ed.* **2019**, *58* (29), 9712–9740. https://doi.org/10.1002/anie.201814441.

(34) Norikane, Y.; Uchida, E.; Tanaka, S.; Fujiwara, K.; Nagai, H.; Akiyama, H. Photoinduced Phase Transitions in Rod-Shaped Azobenzene with Different Alkyl Chain Length. *J. Photopolym. Sci. Technol.* **2016**, *29* (1), 145–148. https://doi.org/10.2494/photopolymer.29.149.

(35) Norikane, Y.; Uchida, E.; Tanaka, S.; Fujiwara, K.; Koyama, E.; Azumi, R.; Akiyama, H.; Kihara, H.; Yoshida, M. Photoinduced Crystal-to-Liquid Phase Transitions of Azobenzene Derivatives and Their Application in Photolithography Processes through a Solid–Liquid Patterning. *Org. Lett.* **2014**, *16* (19), 5012–5015. https://doi.org/10.1021/ol502223u.

(36) Norikane, Y.; Saito, K. Crawling Motion of Crystals on Solid Surfaces by Photo-Induced Reversible Crystal-to-Melt Phase Transition. In *Mechanically Responsive Materials for Soft Robotics*; Wiley-VCH Verlag GmbH & Co. KGaA, 2019; pp 83–103. https://doi.org/10.1002/9783527822201.ch4.

(37) Al-kaysi, R. O. Spontaneous Peeling of Tetragonal Microcrystals with Short Pulses of UV-Light, January 15, 2019.

(38) Tong, F.; Kitagawa, D.; Bushnak, I.; Al-Kaysi, R. O.; Bardeen, C. J. Light-Powered Autonomous Flagella-Like Motion of Molecular Crystal Microwires. *Angew. Chemie - Int. Ed.* **2021**, *60* (5), 2414–2423. https://doi.org/10.1002/anie.202012417.

(39) Tong, F.; Chen, S.; Li, Z.; Liu, M.; Al-Kaysi, R. O.; Mohideen, U.; Yin, Y.; Bardeen, C. J. Crystal-to-Gel Transformation Stimulated by a Solid-State E→Z Photoisomerization. *Angew. Chemie - Int. Ed.* **2019**, *58* (43), 15429–15434. https://doi.org/10.1002/anie.201907454.

(40) Al-Kaysi, R. O.; Zhu, L.; Al-Haidar, M.; Al-Muhannah, M. K.; El-Boubbou, K.; Hamdan, T. M.; Bardeen, C. J. Chemical Reaction Method for Growing Photomechanical Organic Microcrystals. In *CrystEngComm*; Royal Society of Chemistry, 2015; Vol. 17, pp 8835–8842. https://doi.org/10.1039/c4ce02387k.

(41) Ekka, A.; Kurakula, U.; Choudhury, A.; Mishra, A.; Faye, A.; Halcovitch, N. R.; Medishetty, R. Light-Driven Flagella-like Motion of Coordination Compound Single Crystals. *Chem. Commun.* **2023**, *59* (29), 4384–4387. https://doi.org/10.1039/D3CC00333G.

(42) Al-Kaysi, R. O.; Tong, F.; Al-Haidar, M.; Zhu, L.; Bardeen, C. J. Highly Branched Photomechanical Crystals. *Chem. Commun.* **2017**, *53* (17), 2622–2625. https://doi.org/10.1039/C6CC08999B.

(43) Tong, F.; Xu, W.; Al-Haidar, M.; Kitagawa, D.; Al-Kaysi, R. O.; Bardeen, C. J. Photomechanically Induced Magnetic Field Response by Controlling Molecular Orientation in 9-Methylanthracene Microcrystals. *Angew. Chemie - Int. Ed.* **2018**, *57* (24), 7080–7084. https://doi.org/10.1002/anie.201802423.

(44) Xu, T.-Y.; Cui, M.; Zhao, C.; Zhou, S.-W.; Zhang, T.-L.; Lin, H.-Y.; Tong, F.; Qu, D.-H. Visible Light-Induced Collapse of Molecular Microcrystals into Droplets by E-to-Z Photoisomerization and Melting Phase Transition. *CCS Chem.* **2023**, 1–14.

(45) Koibuchi, R.; Omasa, K.; Yoshikawa, I.; Houjou, H. Photoinduced Crystal-to-Liquid Transition of Acylhydrazone-Based Photoswitching Molecules. *J. Phys. Chem. Lett.* **2023**, *14*, 8320–8326.